Magn Reson Med Sci 2018; 17; 174–183
doi:10.2463/mrms.tn.2016-0049
Published Online: March 27, 2017

TECHNICAL NOTE

Spiral MRI on a 9.4T Vertical-bore Superconducting Magnet Using Unshielded and Self-shielded Gradient Coils

Nao Kodama, Ayana Setoi, and Katsumi Kose*

Spiral MRI sequences were developed for a 9.4T vertical standard bore (54 mm) superconducting magnet using unshielded and self-shielded gradient coils. Clear spiral images with 64-shot scan were obtained with the self-shielded gradient coil, but severe shading artifacts were observed for the spiral-scan images acquired with the unshielded gradient coil. This shading artifact was successfully corrected with a phase-correction technique using reference scans that we developed based on eddy current field measurements. We therefore concluded that spiral imaging sequences can be installed even for unshielded gradient coils if phase corrections are performed using the reference scans.

Keywords: *spiral scan, shielded gradient coil, superconducting magnet, eddy current*

Introduction

Spiral MRI sequences have several unique advantages over other MRI sequences, such as efficient data acquisition, flexible k-trajectory design, robustness to flow and motion, and short echo times.[1,2] However, there are many hurdles to be overcome such as very high magnetic field homogeneity, precise gradient waveform design and control, and image reconstruction, and many studies have dealt with spiral MRI since its original demonstration.[3–7]

Recently, we reported on echo-planar imaging (EPI) using an unshielded gradient coil set for a 9.4T standard vertical bore (54 mm) superconducting magnet.[8] In this previous study, the unshielded gradient coil was used to obtain a sufficient sample volume (32 mm diameter bore of the gradient coil) designed for live mouse imaging in the small bore magnet, and the eddy current problems for EPI were overcome by gradient rise-time control and phase corrections using reference scans. Spiral imaging sequences are very sensitive to eddy current fields similar to the EPI sequences, and therefore development of spiral imaging sequences using an unshielded gradient coil in a superconducting magnet is also challenging. To the author's knowledge, there have been no studies that have reported spiral imaging using an unshielded gradient coil in a superconducting magnet to date.

In this study, we developed a phase correction technique for spiral-scan images based on eddy current measurements and reference scans, and we successfully obtained spiral-scan images with the unshielded gradient coil that were as clear as those acquired with the self-shielded gradient coil.

Institute of Applied Physics, University of Tsukuba, 1-1-1 Tennodai, Tsukuba, Ibaraki 305-8573, Japan

*Corresponding author, Phone: +81-298-53-7274, Fax: +81-298-53-5205, E-mail: kose@bk.tsukuba.ac.jp

Received: May 5, 2016 | Accepted: February 1, 2017

Materials and Methods

MRI system using a 9.4T vertical-bore superconducting magnet

The MRI system consisted of a 9.4T vertical-bore superconducting magnet, a home-built room-temperature shim coil, two exchangeable gradient coil sets, a radio-frequency (RF) coil, and a digital MRI console. The superconducting magnet (JMTC-400/54/SS, JASTEC, Kobe, Japan) had a 54 mm diameter room-temperature bore and the homogeneity was about 1 ppm over 17 mm in diameter and 36 mm long central ellipsoidal volume. The room-temperature shim coil consisted of five second-order coil elements wound over an acrylic pipe (outer diameter [o.d.] = 44 mm, inner diameter [i.d.] = 40 mm) using 0.4 mm diameter polyurethane coated Cu wire. We used both unshielded and self-shielded exchangeable gradient coil sets (MRTechnology Inc., Tskukuba, Japan) as shown in Fig. 1. For the unshielded gradient coil, the o.d. and i.d. were 39 and 32 mm, and the efficiencies were 19.0, 19.2, and 33.7 mT/m/A for Gx, Gy, and Gz, respectively. For the self-shielded gradient coil, the o.d. and i.d. were 39 and 24 mm and the efficiencies were 23.3, 24.1, and 26.6 mT/m/A for Gx, Gy, and Gz, respectively. The RF coil was a home-built saddle-shaped coil (14 mm

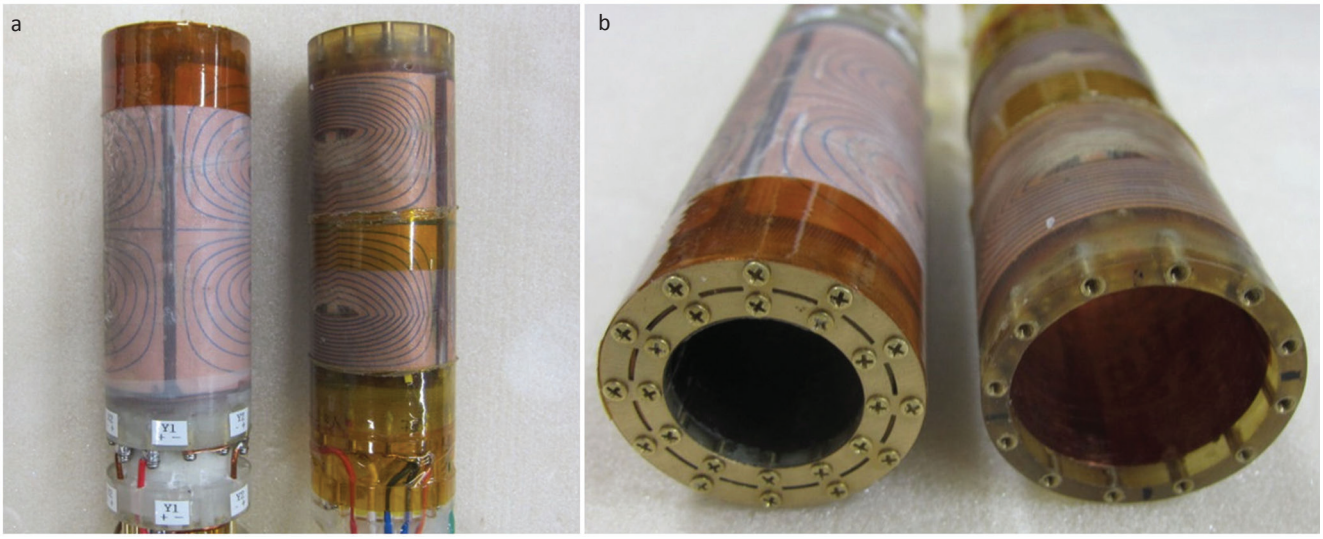

Fig. 1 Self-shielded and unshielded gradient coils for the 9.4T vertical bore superconducting magnet. (**a**) Side view, self-shielded (left) and unshielded (right). (**b**) Top view, self-shielded (left) and unshielded (right). The bore diameters are 32 and 24 mm for the unshielded and self-shielded gradient coils, respectively.

diameter and 22 mm long). The MRI system was controlled by a digital MRI console with a 128-bit word length and 1 μs time-resolution pulse sequence controller.[9]

Configuration of metallic conductors affecting eddy currents in the magnet

The cryostat of the 9.4T standard bore superconducting magnet was composed of three copper tubes and one aluminum tube. The copper tubes were used for the room temperature bore and cryogen vessels, and their temperatures were room temperature, liquid nitrogen temperature (77 K), and liquid helium temperature (4.2 K). The inner diameters of the copper tubes were 53.84, 61.14, and 69.74 mm, and their lengths were 971, 797, and 684 mm, respectively. The thickness of all the copper tubes was 1.63 mm. The aluminum tube was used for a bobbin for the superconducting wire. The inner diameter, length, and thickness of the aluminum tube were 81.1, 410, and 3.0 mm, respectively.

The gradient coil sets had a few tens of micrometer thick cylindrical copper RF shields just inside the bore. The saddle shaped RF coil had another cylindrical copper RF shield. The outer diameter, length, and thickness of the RF shield were 22, 78, and 0.1 mm, respectively.

Measurements of eddy current magnetic fields generated by the gradient coils

When time-varying electric currents are flowing through gradient coils, eddy currents are induced in the surrounding conducting parts in the magnet. The eddy currents produce eddy current magnetic fields that vary with time. The eddy current magnetic fields consist of various spatial components with different spatial symmetries usually represented by spherical harmonic functions. Among the spatial components of the eddy current magnetic fields, the dominant ones are the spatially uniform components called "B_0 eddy fields" and the spatially linearly changing components called "linear eddy fields."[10]

To measure the B_0 eddy and the linear eddy fields, we placed a water phantom made of a plastic sphere (o.d. = 10 mm, i.d. = 8 mm) filled with $CuSO_4$ water solution at the center of the gradient coils in the magnet and used the pulse sequence shown in Fig. 2. In this pulse sequence, a gradient pulse with 100 ms duration time was applied at the beginning, and a square RF pulse (pulse width = 24 μs) was applied after a delay time t_{RF} from the falling edge of the gradient pulse. The free induction decay (FID) signal was affected by the linear eddy and the B_0 eddy fields as shown in Fig. 2. The effects of the eddy fields were detected using the gradient echo signal observed 19.36 ms after the application of the RF pulse. The gradient echo signal was repeatedly acquired as the gradient coil current was changed from −5.000 to +4.844 A in 64 steps. The linear eddy fields were calculated from the positional shift Δt of the gradient echo peak, and the B_0 eddy fields were calculated from the phase shift of the gradient echo peak. The linear eddy and the B_0 eddy fields measured as the functions of t_{RF}, which was changed from 0.01 to 100 ms by 52 steps, were decomposed into three exponentially decaying components with different time constants and different amplitudes.

Pulse sequence design and the image reconstruction method

The spiral gradient waveforms were designed using the analytical solution developed by Glover.[3] The image matrix was 128 × 128 pixels, and the number of shots was 2, 4, 8, 16, 32, and 64; the data acquisition times for the one shot scan were 75.58,

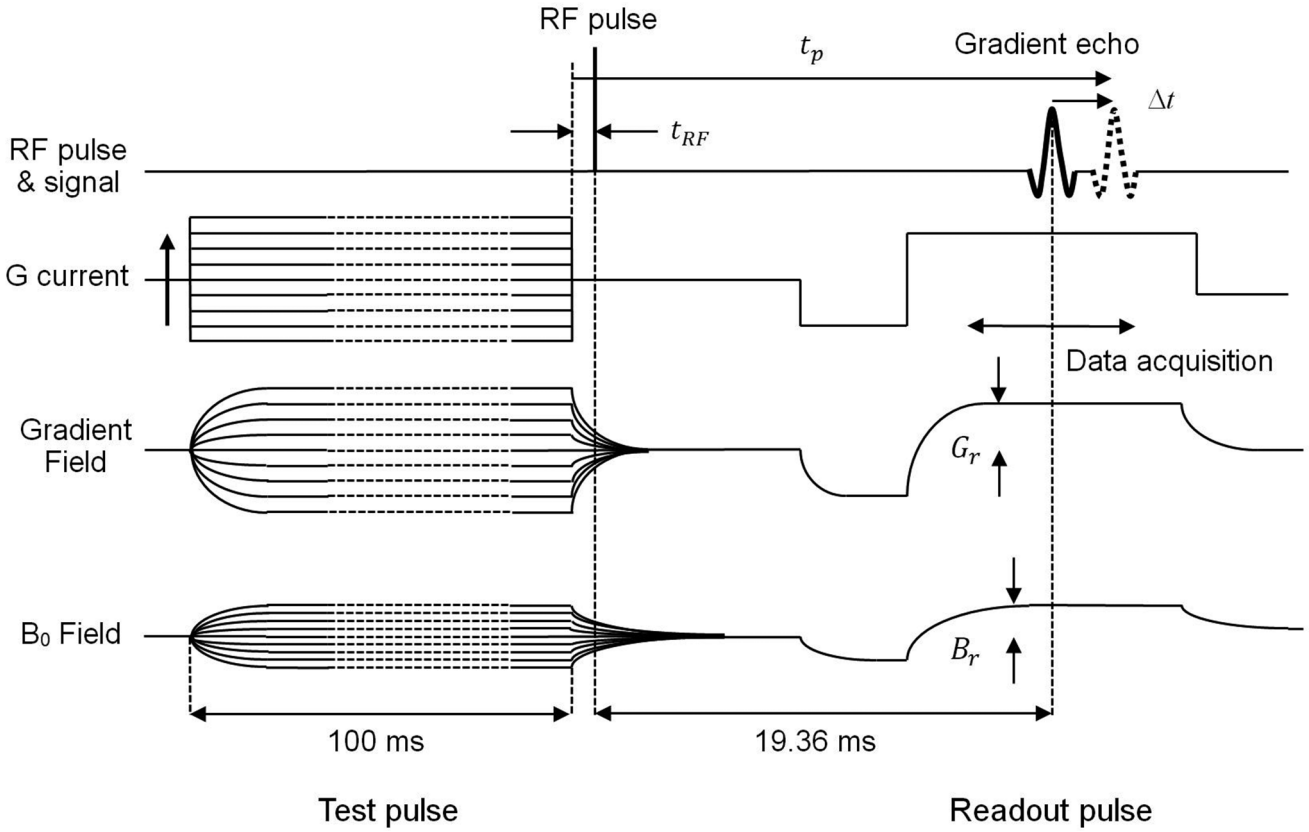

Fig. 2 Pulse sequence to measure the linear eddy fields and the B_0 eddy fields. G_r and B_r are amplitudes of the readout field gradient and applied homogeneous field. The current of the gradient coil was changed from −5.00 A to +4.844 A in 64 steps. The time t_{RF} was changed from 0.01 to 100 ms by 52 steps. RF, radio-frequency.

37.79, 19.14, 9.57, 4.79, and 2.39 ms, respectively. The slice thickness was 2 mm, and the FOV was 15.36 mm × 15.36 mm. Because TR of one-shot spiral data acquisition was 400 ms, the total data acquisition times were 0.8, 1.6, 3.2, 6.4, 12.8, and 25.6 s for 2-, 4-, 8-, 16-, 32-, and 64-shot spiral sequences, respectively. The pulse sequences and k-trajectories developed for 64- and 8-shot spiral data acquisition are shown in Fig. 3. We used a water phantom made of 19 glass capillaries (o.d. = 1.4 mm, i.d. = 0.9 mm, length = 120 mm) in an nuclear magnetic resonance (NMR) sample tube (o.d. = 10.0 mm, i.d. = 9.0 mm, length = 130 mm) filled with $CuSO_4$ doped water solution ($T_1 \sim 200$ ms).

For comparison, we used a two dimensional (2D) spin-echo Fourier imaging sequence with TR = 400 ms, TE = 80 ms, data-acquisition window = 64 ms, image matrix = 256 × 256, slice thickness = 2 mm, and FOV = 15.36 mm × 15.36 mm, and one-shot 2D EPI sequences using Gx and Gy readout gradients with TR = 400 ms, TE = 80 ms, data-acquisition window = 64 ms, image matrix = 64 × 64, slice thickness = 2 mm, and FOV = 15.36 mm × 15.36 mm. These images were measured using the unshielded gradient coil.

Image reconstruction was performed using the 2D Fourier transform after nearest neighbor gridding and convolution gridding methods using a Gaussian convolution kernel.[2,11]

Phase correction using the reference scan

To measure phase shifts of the NMR signal caused by the eddy current fields, we acquired the NMR signal using the spiral imaging sequences with Gx or Gy switched off. In these reference scans, the k-trajectories oscillated on the k_x or k_y axes and repeatedly passed through the k-space origin (Fig. 4). Therefore, large NMR signal peaks were repeatedly observed when the k-trajectory passed through the k-space origin. We detected the peak positions and calculated the phase of the NMR signals at the peak positions observed at the k-space origin.

Results

Eddy current magnetic fields measured for the gradient coils

Tables 1 and 2 show time constants and relative amplitudes, the ratio of the amplitude of the linear eddy fields to that of applied gradient fields, of two major exponentially decaying components of the linear eddy fields measured for the unshielded and the self-shielded gradient coils. In Table 1,

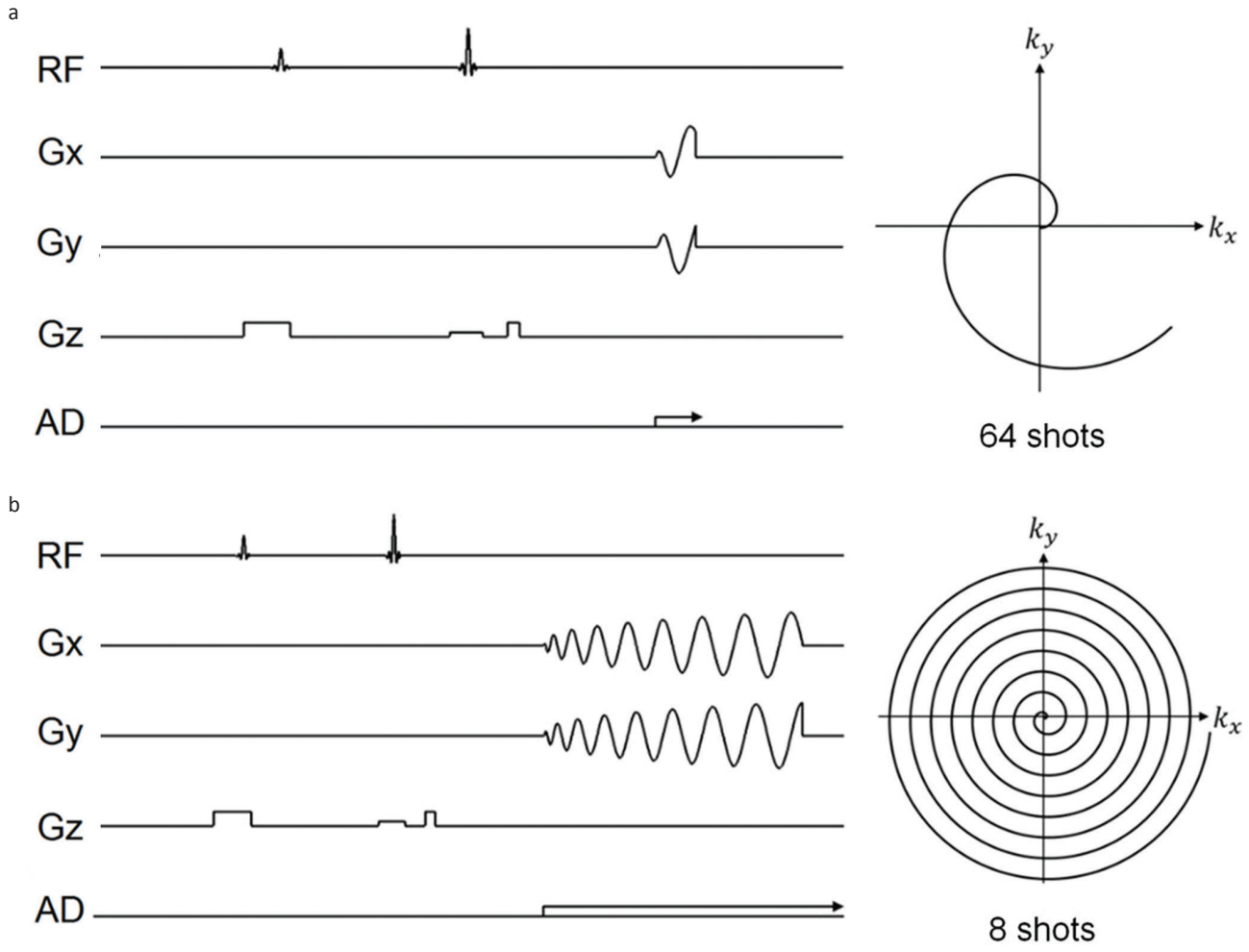

Fig. 3 Pulse sequences and k-trajectories for the multishot spiral imaging sequences. (**a**) 64 shots. (**b**) 8 shots. Only one trajectory is displayed in the k-space. RF, radio-frequency.

the components of the linear eddy fields for the unshielded gradient coil are categorized into two groups: one group with time constants of about 0.3 ms and relative amplitudes of 25−38% and another with time constants of about 7 ms and relative amplitudes of 7−11%. In Table 2, the components of the linear eddy fields for the shielded gradient coil are categorized into major two groups: one group with time constants of about 0.05 ms (50 μs) and relative amplitudes of about 60% and another with time constants of about 0.3−0.45 ms and relative amplitudes of 1.1−2.4%. The amplitude of the linear eddy field components with time constants of about 0.3 ms reduced from 25−38% to 1.1−2.4% from the unshielded to the self-shielded gradient coil, clearly demonstrating that the linear eddy fields were drastically reduced from the unshielded to the self-shielded gradient coil.

Tables 3 and 4 show the time constants and amplitudes of two major exponentially decaying components of the B_0 eddy fields measured for the unshielded and the self-shielded gradient coils. The B_0 eddy fields were normalized by those produced by the gradient switching of 1 T/m/s. The temporal changes of the B_0 eddy fields measured for the unshielded and self-shielded gradient coils are shown in Fig. 5. It is remarkable that the unshielded Gy gradient coil induced a large B_0 field with a very short time constant (~84 μs).

MR images of a water phantom

Figure 6 shows 2D cross sections of the water phantom acquired with the 2D spin-echo Fourier imaging sequence (a), the EPI sequence with the unshielded Gx readout gradient (b), and that with the unshielded Gy readout gradient (c). Because the pixel bandwidth was 15.625 Hz (~0.04 ppm for the 400 MHz resonance frequency) in Fig. 6(a) and the magnetic field inhomogeneity caused a positional shift along the readout direction (horizontal direction) at each point, this MR image suggested that the magnetic field homogeneity in this plane was of the order of 0.1 ppm. This is because the positional shift of the 2D spin-echo image seemed less than three or four pixel lengths

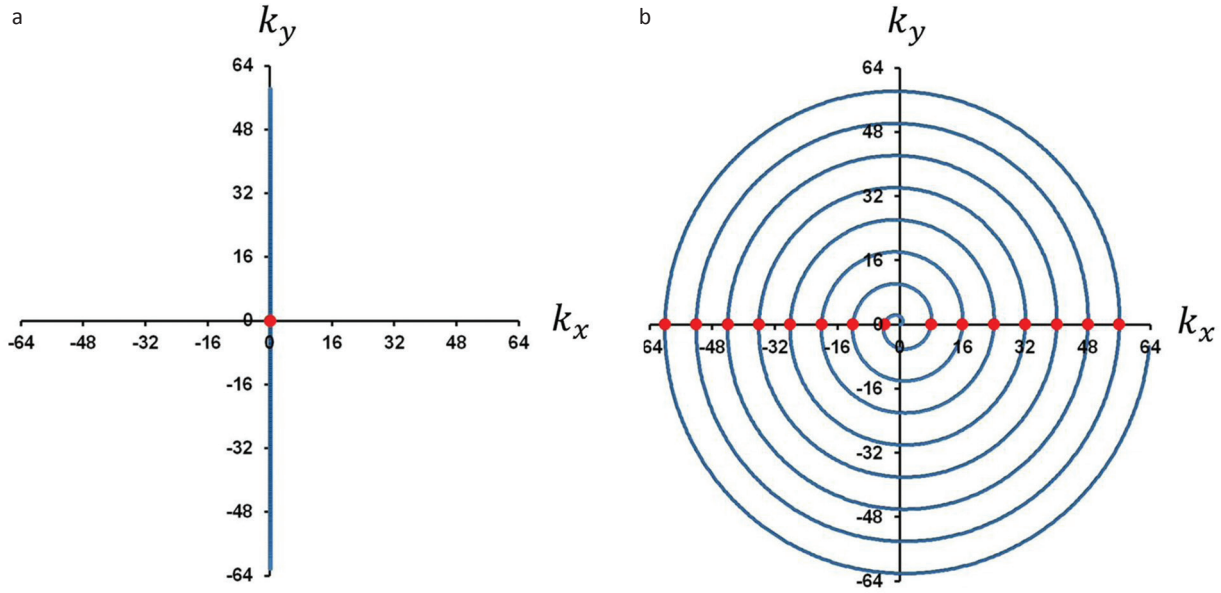

Fig. 4 (**a**) The k-trajectory of the reference scan for one of the 8-shot spiral scan with Gx OFF and Gy ON. At the center of the k-space, large echo signals are repeatedly observed; (**b**) k-trajectory for one of the 8-shot spiral scan. The echo peaks observed in (**a**) correspond to the positions marked as the circles on the k_x axis.

Table 1. Time constants and relative amplitudes of the linear eddy fields observed for the unshielded gradient coils. The relative amplitude is the ratio of the amplitude of the linear eddy fields to that of applied gradient field

	Gx		Gy		Gz	
	Component 1	Component 2	Component 1	Component 2	Component 1	Component 2
Time constant [ms]	0.27	6.6	0.28	6.8	0.26	7.0
Relative amplitude [%]	38.4	10.7	30.1	8.90	24.9	6.99

Table 2. Time constants and amplitudes of the linear eddy fields observed for the self-shielded gradient coils. The relative amplitude is the ratio of the amplitude of the linear eddy fields to that of applied gradient field

	Gx		Gy		Gz	
	Component 1	Component 2	Component 1	Component 2	Component 1	Component 2
Time constant [ms]	0.053	0.29	0.054	0.46	0.048	0.30
Relative amplitude [%]	61.0	1.62	56.4	1.09	61.4	2.39

along the readout direction. The EPI images also demonstrated that the homogeneity of the magnetic field was of the order of 0.1 ppm in this plane because the magnetic field inhomogeneity caused a positional shift along the phase encoding direction (vertical direction) at each point. This is because the positional shift of the EPI image seemed less than three or four pixel lengths along the phase encoding direction.

Spiral-scan images acquired with the self-shielded gradient coil reconstructed using both the nearest neighbor gridding method and the convolution gridding method for 64-, 32-, 16-, 8-, 4-, and 2-shot scans are presented in Fig. 7. Although neither image distortion nor phase distortion was observed for these spiral images, reconstruction noise (artifact) specific to the gridding methods was observed over the reconstructed images. In addition, serious image blurring caused by the magnetic field inhomogeneity in the slicing plane was observed for fewer-shot (2−16-shot) images.

Spiral-scan images acquired with the self-shielded gradient coil and the unshielded gradient coil for 64-, 32-, 16-, 8-, 4-, and 2-shot scans and reconstructed with the nearest neighbor gridding method are shown in Fig. 8. The spiral images acquired with the unshielded gradient coil have severe intensity shading compared with those acquired with the self-shielded gradient coil, which was considered to be caused by the B_0 eddy fields of the gradient coil.

Table 3. B_0 eddy field measured for the unshielded gradient coil. The amplitude is normalized by the amplitude for the gradient field switching of 1 T/m/s

	Gx		Gy		Gz	
	Component 1	Component 2	Component 1	Component 2	Component 1	Component 2
Time constant [ms]	0.84	11.6	0.084	12.6	0.048	7.26
Amplitude [μT/(T/m)]	183	−7.4	−1766	7.68	128	65.8

Table 4. B_0 eddy field measured for the self-shielded gradient coil. The amplitude is normalized by the amplitude for the gradient field switching of 1 T/m/s

	Gx		Gy		Gz	
	Component 1	Component 2	Component 1	Component 2	Component 1	Component 2
Time constant [ms]	1.92	21.8	10.4	63	0.2	5.25
Amplitude [μT/(T/m)]	14.2	−4.3	−12.3	2.14	324	50.4

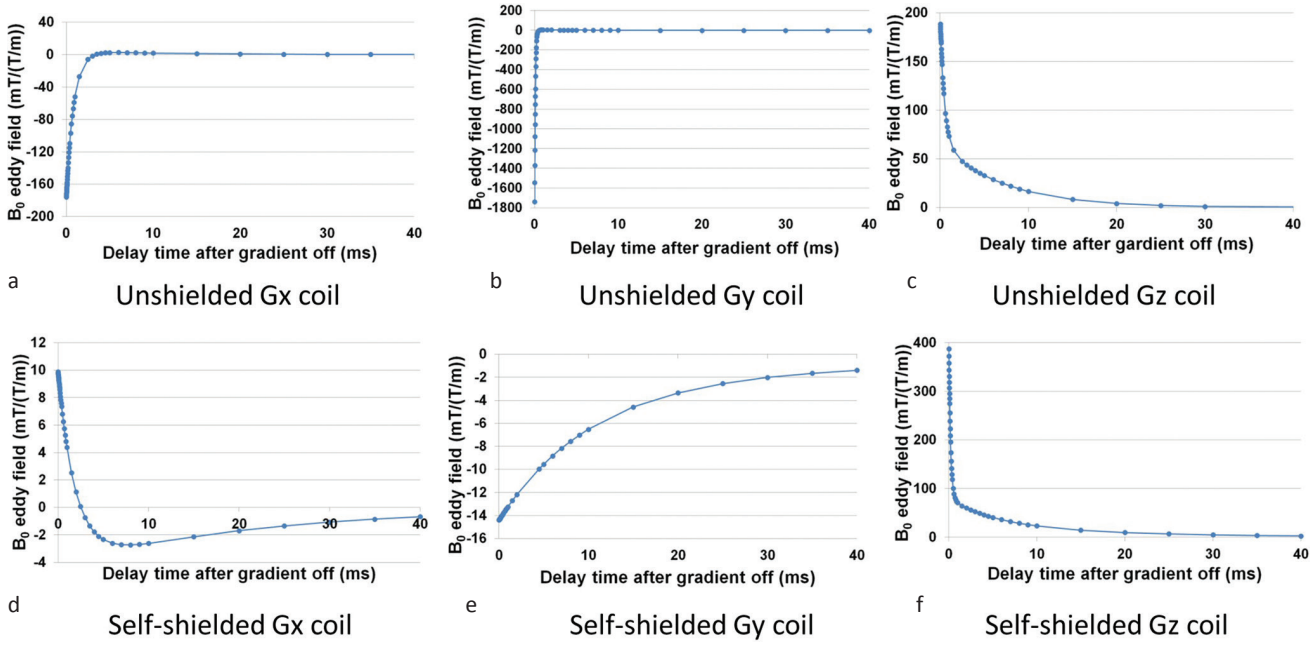

Fig. 5 Temporal change of B_0 eddy fields measured after the gradient pulses. (**a**), (**b**), and (**c**) are B_0 eddy fields for the unshielded gradient coil of Gx, Gy, and Gz. (**d**), (**e**), and (**f**) are B_0 eddy fields for the self-shielded gradient coil of Gx, Gy, and Gz, resepectively.

Phase correction using the reference scan

Figure 9 presents the phase shift calculated from the echo peak signal of the reference scan and the shape of the gradient coil current for the Gx gradient field (a) and the Gy gradient field (b) for the unshielded gradient coil. The agreement between the detected phase shift (red circles) and the shape of the gradient coil current (blue line) is very good for Gy. However, the agreement is not so good for Gx.

The uncorrected and corrected spiral images acquired with the unshielded gradient coil are shown in Fig. 10. The phase correction was performed only for the Gy gradient coil current because the phase shift caused by the Gx gradient coil current was relatively small (~1/30 of that of Gy). Although the phase correction was not perfect, the severe intensity shading of the images acquired with 64- and 8-shots was well corrected and that acquired with other shots was slightly corrected.

Effects of linear eddy fields

The spiral images acquired with both gradient coils for 64-shot sequences and 8-shot sequence for the unshielded gradient coil are shown in Fig. 11. It is clear from these images that the image size was reduced because of eddy current effects: about 89% (horizontally) and 92% (vertically) of the designed size with the self-shielded gradient coil, about

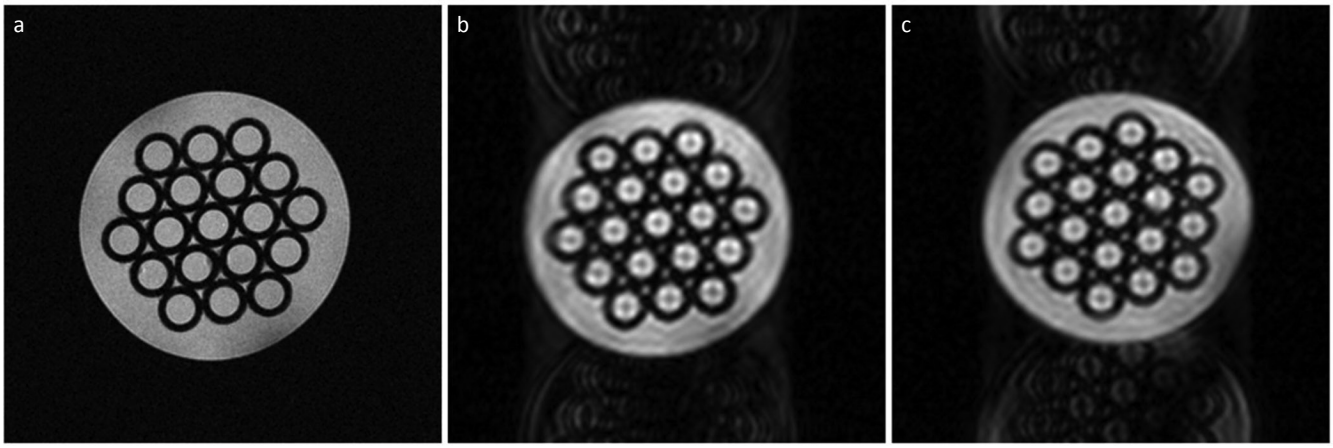

Fig. 6 Two-dimensional cross section of a water phantom acquired with (**a**) a spin-echo Fourier imaging sequence, (**b**) an echo-planar imaging (EPI) sequence with the Gx readout gradient, and (**c**) an EPI sequence with the Gy readout gradient.

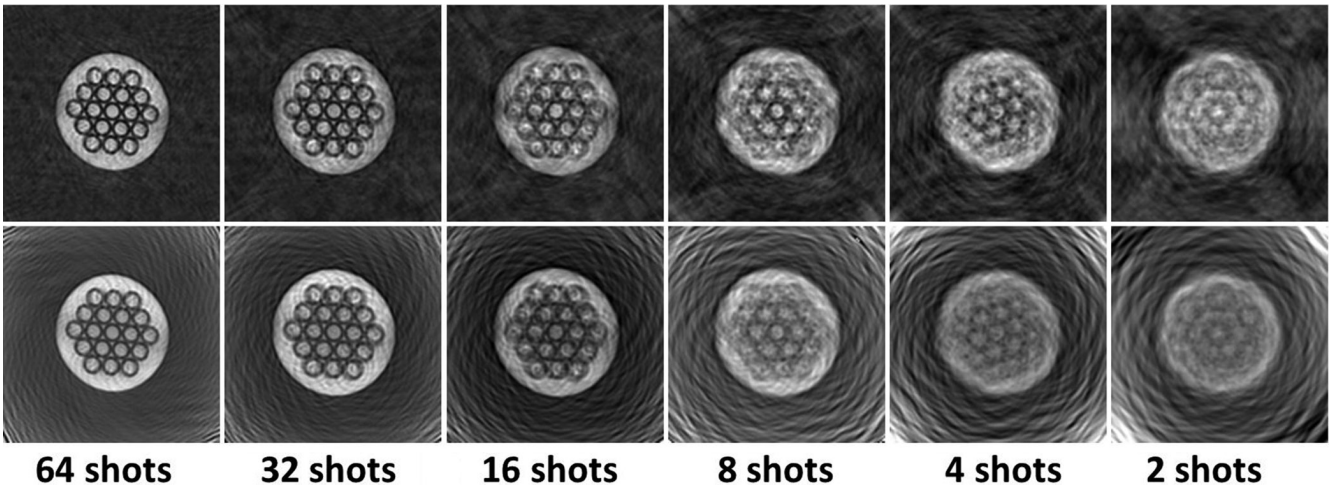

Fig. 7 Spiral images acquired with the self-shielded gradient coil reconstructed using the nearest neighbor gridding method (upper) and the convolution gridding method (lower). The numbers of the shots are displayed under the images. Real part images are shown.

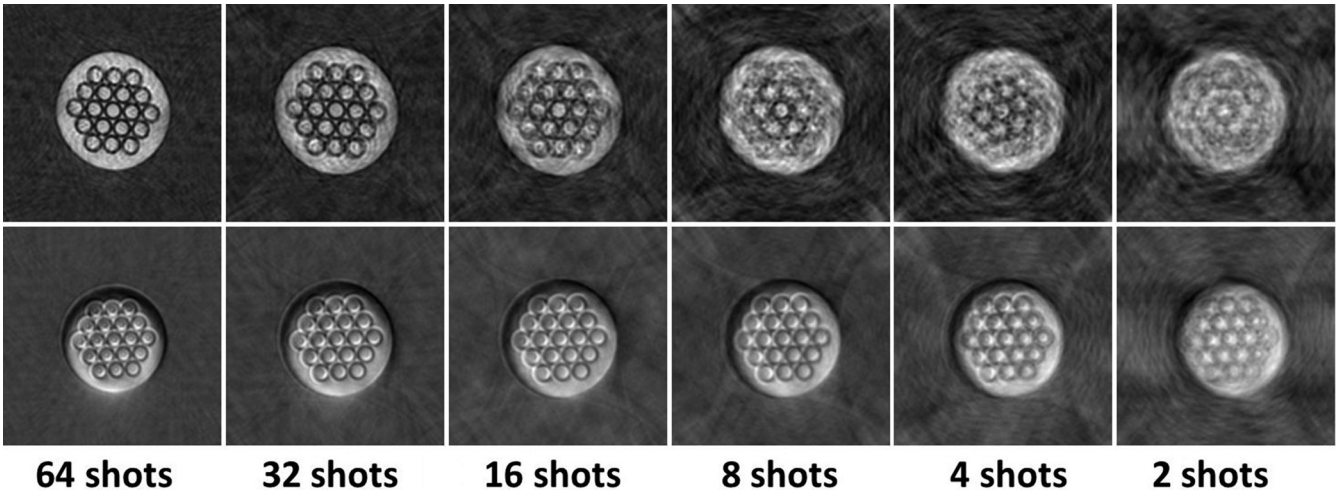

Fig. 8 Multishot spiral images acquired with the self-shielded gradient coil (upper) and the unshielded gradient coil (lower) reconstructed using the nearest neighbor gridding method. Real part images are shown.

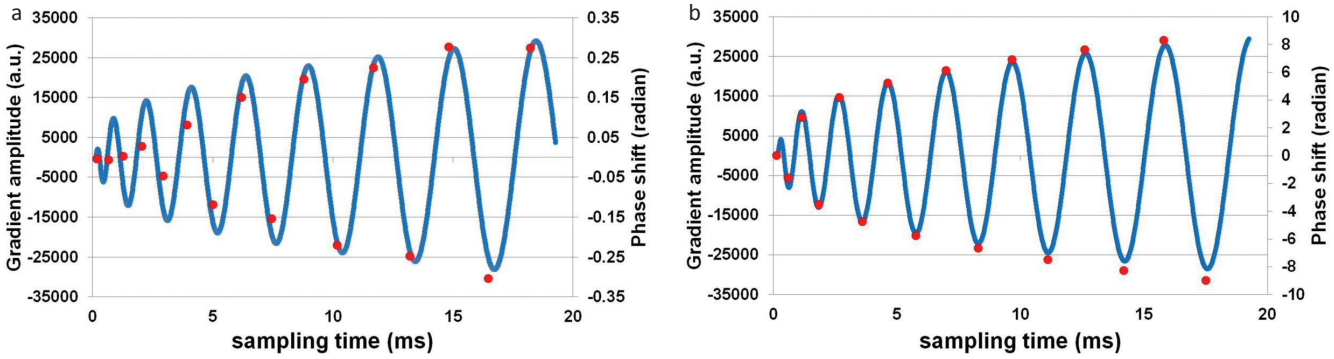

Fig. 9 Signal peak phase observed in the reference scan plotted together with the gradient waveform for the 8-shot spiral scan. The signal phase is plotted as circles, and the gradient waveform is drawn by the curves. (**a**) The reference scan with Gx ON and Gy OFF. (**b**) The reference scan with Gx OFF and Gy ON. The phase shift caused by the Gy gradient coil is much larger than that caused by the Gx gradient coil.

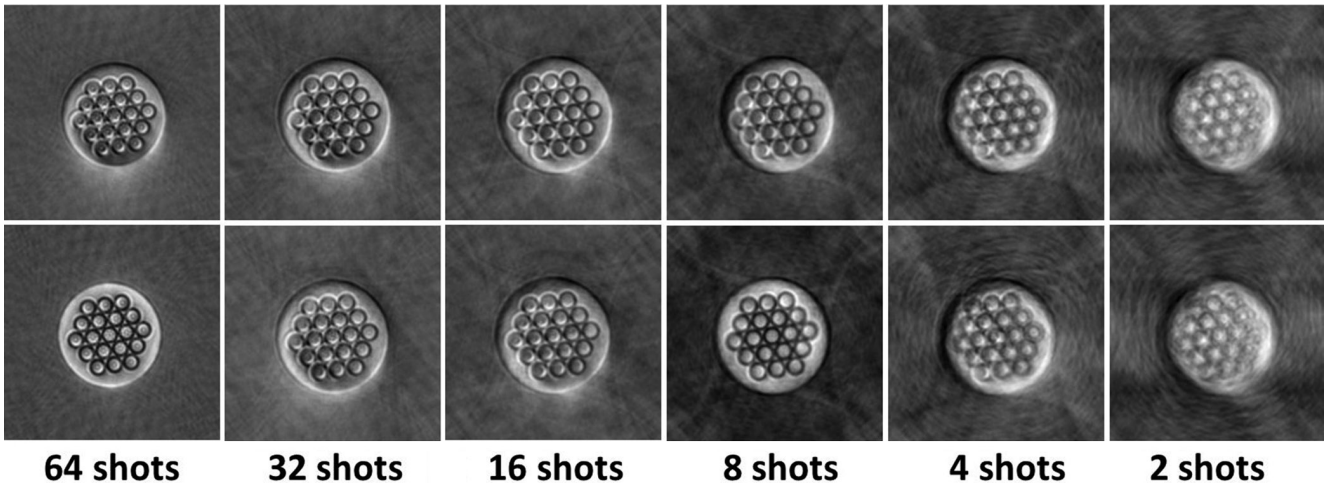

Fig. 10 Multishot spiral images acquired with the unshielded gradient coil. With (lower row) and without (upper low) phase correction. These images were reconstructed using the nearest neighbor gridding method. The upper figures are identical to the lower figures in Fig.8. Real part images are shown.

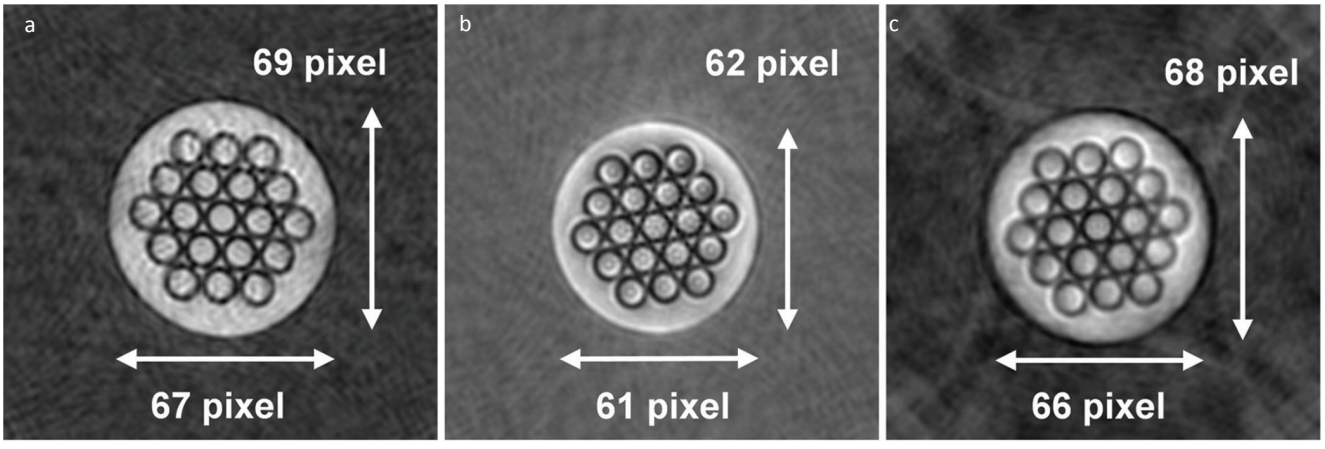

Fig. 11 Multishot spiral images acquired with both gradient coils for 64-shot sequences (**a**): self-shielded, (**b**): unshielded) and 8-shot sequence for the unshielded gradient coil (**c**). The image acquired with the unshielded gradient coil was corrected by the phase shift measured using the reference scan. The image size of (**a**) is about 89% and 92%, and that of (**b**) is about 81% and 83%, and that of (**c**) is about 88% and 91% of the designed image size, for the horizontal and the vertical direction of the images, respectively. The image size reduction was caused by the linear eddy fields induced by the time variation of the readout gradients, Gx and Gy.

81% (horizontally) and 83% (vertically) of the designed size for the 64-shot sequence with the unshielded coil, and 88% (horizontally) and 91% (vertically) of the designed size for the 8-shot sequence with the unshielded gradient coil.

Discussion

Eddy current fields caused by the gradient coil current switching

The linear eddy fields could be decomposed into three components, and of these, the two major ones were tabulated (Tables 1 and 2). Because the shielded gradient was designed to cancel the gradient magnetic field on the surface of the room temperature magnet bore (diameter = 54 mm), the linear eddy field components with about 0.3 ms time constants, which were reduced by about 10–30 times, were considered to be induced on the room temperature magnet bore. This result clearly demonstrated that the shielding efficiency was higher than 90%. Because the thickness of the room temperature copper tube was 1.63 mm, most of the eddy currents induced outside of the gradient coils were considered to be produced by the room temperature bore tube.

However, very large linear eddy fields with short time constants (~ 50 μs) were observed for the self-shielded gradient coil. We think that these eddy current fields were induced in the RF shield (a few tens of micrometers thick Cu sheet) wound inside of the self-shielded gradient coil and that (100 micrometer thick Cu sheet) wound outside of the RF probe, because the conductors with lower conductivity produce shorter decaying time constants of the eddy currents. However, because the time constant of this linear eddy field component was very short, the effect of this eddy field component on the slew rate of the gradient field was small.

The amplitudes of the B_0 eddy fields caused by Gx and Gy for the unshielded gradient coil were 10–100 times larger than those for the self-shielded coil (Tables 3 and 4). We think that this result is essential for the severe shading artifact observed in spiral images acquired with the unshielded gradient coil.

Phase correction using the reference scan

In general, eddy fields generated by the applied field gradient, proportional to the gradient coil current , can be calculated using convolution integral of the step response of the eddy fields and the time derivative of the gradient coil current. However, if the time constant of the eddy field component is very short (*e.g.* tens of microsecond for B_0 eddy field by Gy of the unshielded gradient, much shorter than the rotational cycle of the spiral trajectory [~2 ms]), the step response of the eddy fields can be approximated as the delta function and the convolution integral can be approximated to be time derivative of the gradient coil current. Therefore, in this case, the B_0 eddy field ΔB_0(t) can be written as,

$$\Delta B_0(t) \cong \alpha \frac{dI(t)}{dt},$$

where α is a proportionality constant.

The angular frequency shift of the NMR signal caused by the B_0 eddy field is, and thus the phase shift $\Delta\Phi$(t) caused by the B_0 eddy field is

$$\Delta\phi(t) = \int_0^t \gamma \Delta B_0(u)du \cong \gamma \int_0^t \alpha \frac{dI(u)}{du} du = \alpha\gamma[I(u)]_0^t = \alpha\gamma I(t),$$

because I(0) = 0 for the spiral imaging sequences used in this study. This equation shows that the phase shift caused by the B_0 eddy field is proportional to the waveform of the gradient coil current.

As described in "Results" section, Fig. 9 shows the phase shift calculated from the echo peak signal of the reference scan and the shape of the gradient coil current I(t) for the Gx gradient field (a) and the Gy gradient field (b) for the unshielded gradient coil. The agreement between the detected phase shift and the shape of the gradient coil current is very good for Gy, which justifies the above equation for the unshielded gradient coil. However, the agreement is not so good for Gx. This is because the time constant 0.84 ms of the primary component of the B_0 eddy field caused by Gx is about 10 times larger than the time constant 0.084 ms of that caused by Gy. Therefore, the assumption that the time constant of the B_0 eddy field component is much smaller than the rotational cycle of the spiral trajectory (~2 ms) is not valid for Gx but valid for Gy. This is the reason for the difference of the agreement between Fig. 9a and b. Therefore, the phase of the NMR signal acquired with the spiral sequence can be corrected using the gradient coil current calibrated by the phase shift measured using the reference scan.

As shown in Fig. 10, the severe intensity shading of the images acquired with 64- and 8-shots was well corrected and that acquired with other shots was only slightly corrected. Although the reason why the intensity shading of the 8-shot image was well corrected was unclear, this result demonstrated the correctness of our approach.

Linear eddy field effects on the spiral scan images

The effect of the linear eddy fields on the spiral images is the reduction in image size (Fig. 11), because these eddy fields reduce the intensity of the gradient fields. Although the exact calculation of the field gradient amplitude using the linear eddy fields needs convolution integral of the time derivative of the gradient waveform and the step response of the linear eddy fields, the image size reduction can be understood qualitatively using the intensity of the linear eddy fields tabulated Tables 1 and 2.

Conclusion

We developed spiral-imaging sequences for a 9.4T standard vertical bore (54 mm) superconducting magnet using unshielded and self-shielded gradient coils. Although spiral

images acquired with the self-shielded gradient coil using 64-shot scans showed no noticeable artifact, those acquired with the unshielded gradient coil showed a severe intensity-shading artifact, which was successfully corrected with the phase correction technique that we developed in this study using reference scans. We therefore conclude that spiral imaging sequences can be installed even with an unshielded gradient coil if we perform phase corrections using the reference scan.

Acknowledgments

We acknowledge Drs. Tomoyuki Haishi and Seitaro Hashimoto for the development of the 9.4T superconducting MRI system. We also thank Mr. Ryoichi Kose for providing the image reconstruction program using the convolution gridding and Mr. Yuta Kobayashi for analyzing the eddy current measurements. This work was supported by the System Development Program for Advanced Measurement and Analysis Project of the Japan Science and Technology Agency.

Conflicts of Interest

The authors declare that they have no conflicts of interest.

References

1. Ahn CB, Kim JH, Cho ZH. High-speed spiral-scan echo planar NMR imaging-I. IEEE Trans Med Imaging 1986; 5:2–7.
2. Bernstein MA, King KF, Zhou XJ, Handbook of MRI pulse sequences, Burlington MA, Elsevier Academic Press, 2004; 928–954.
3. Glover GH. Simple analytic spiral k-space algorithm. Magn Reson Med 1999; 42:412–415.
4. Tan H, Meyer CH. Estimation of k-space trajectories in spiral MRI. Magn Reson Med 2009; 61:1396–1404.
5. Qian Y, Zhao T, Hue YK, Ibrahim TS, Boada FE. High-resolution spiral imaging on a whole-body 7T scanner with minimized image blurring. Magn Reson Med 2010; 63:543–552.
6. Addy NO, Wu HH, Nishimura DG. Simple Method for MR gradient system characterization and k-Space trajectory estimation. Magn Reson Med 2012;68:120–129.
7. Bhavsar PS, Zwart NR, Pipe JG. Fast, variable system delay correction for spiral MRI. Magn Reson Med 2014; 71:773–782.
8. Kodama N, Kose K. Echo-planar imaging for a 9.4Tesla vertical-bore superconducting magnet using an unshielded gradient coil. Magn Reson Med Sci 2016; 15:395–404.
9. Hashimoto S, Kose K, Haishi T. Development of a pulse programmer for magnetic resonance imaging using a personal computer and a high-speed digital input-output board. Rev Sci Instrum 2012; 83:053702.
10. Bernstein MA, King KF, Zhou XJ, Handbook of MRI pulse sequences, Burlington MA, Elsevier Academic Press, 2004; 316–331.
11. Jackson JI, Meyer CH, Nishimura DG, Macovski A. Selection of a convolution function for Fourier inversion using gridding [computerized tomography application]. IEEE Trans Med Imaging 1991; 10:473–478.